

Generation of sub-MHz and spectrally-bright biphotons from hot atomic vapors with a phase mismatch-free scheme

Chia-Yu Hsu¹, Yu-Sheng Wang¹, Jia-Mou Chen¹, Fu-Chen Huang¹, Yi-Ting Ke¹, Emily Kay Huang¹, Weilun Hung¹, Kai-Lin Chao¹, Shih-Si Hsiao¹, Yi-Hsin Chen^{2,5}, Chih-Sung Chuu^{1,5}, Ying-Cheng Chen^{3,5}, Yong-Fan Chen^{4,5}, and Ite A. Yu^{1,5,*}

¹*Department of Physics, National Tsing Hua University, Hsinchu 30013, Taiwan*

²*Department of Physics, National Sun Yat-Sen University, Kaohsiung 80424, Taiwan*

³*Institute of Atomic and Molecular Sciences,*

Academia Sinica, Taipei 10617, Taiwan

⁴*Department of Physics, National Cheng Kung University, Tainan 70101, Taiwan*

⁵*Center for Quantum Technology, Hsinchu 30013, Taiwan*

Abstract

We utilized the all-copropagating scheme, which maintains the phase-match condition, in the spontaneous four-wave mixing (SFWM) process to generate biphotons from a hot atomic vapor. The scheme enables our biphotons not only to surpass those in the previous works of hot-atom SFWM, but also to compete with the biphotons that are generated by either the cold-atom SFWM or the cavity-assisted spontaneous parametric down conversion. The biphoton linewidth in this work is tunable for an order of magnitude. As we tuned the linewidth to 610 kHz, the maximum two-photon correlation function, $g_{s,as}^{(2)}$, of the biphotons is 42. This $g_{s,as}^{(2)}$ violates the Cauchy-Schwartz inequality for classical light by 440 folds, and demonstrates that the biphotons have a high purity. The generation rate per linewidth of the 610-kHz biphoton source is 1,500 pairs/(s·MHz), which is the best result of all the sub-MHz biphoton sources in the literature. By increasing the pump power by 16 folds, we further enhanced the generation rate per linewidth to 2.3×10^4 pairs/(s·MHz), while the maximum $g_{s,as}^{(2)}$ became 6.7. In addition, we are able to tune the linewidth down to 290 ± 20 kHz. This is the narrowest linewidth to date, among all the various kinds of single-mode biphotons.

*Electronic address: yu@phys.nthu.edu.tw

I. INTRODUCTION

Photons are superior carriers of information and can keep the carried information intact during the transmission, as they never collide with each other and hardly interact with the environment. Single photons are qubits in long-distance quantum communication [1–5]. The biphoton is a pair of single photons. After the first photon of a biphoton pair is detected to start or trigger a quantum operation as the messenger, the second one in the same pair can be conveniently employed in the operation as the heralded qubit. To generate biphotons, the mechanisms of spontaneous parametric down conversion (SPDC) in nonlinear crystals [6–8] and spontaneous four-wave mixing (SFWM) in atomic vapors [9–11] are commonly used.

The photonic qubits of narrower linewidths can enable quantum components, such as quantum memories, quantum wavelength converters, and quantum phase gates, to have higher efficiencies or success rates [12–24]. The SPDC generation can be assisted with an optical cavity to narrow down the linewidth of single photons [25–38]. On the other hand, since the decoherence rate (or coherence time) is typically low (or long) in the cold-atom system, one can also utilize cold atoms in the SFWM process to produce narrow-linewidth biphotons [9, 39–49]. The SFWM has two types of transition schemes: a double- Λ and a ladder schemes. The former is able to produce biphotons with a linewidth of less than 1 MHz [44, 45]. All the biphotons generated by the latter, in either cold- or hot-atom systems, have linewidths of larger than 10 MHz [50–56]. Thus, we only focus on the SFWM of the double- Λ transition scheme in this study.

To date, four groups have reported sources of sub-MHz biphotons. Two groups produced the biphotons with the cavity-assisted SPDC. In Refs. [34, 38], their biphotons had linewidths of 430 and 265 kHz, and generation rates per linewidth were about 88 and 324 pairs/(s·MHz), respectively. Due to the optical cavities, these biphotons are multi-mode and their frequency modes can span a few hundred MHz. The above linewidth and generation rate per linewidth refer to the values of a single frequency mode. Please note that some designs of the SPDC's optical cavity can make single-mode biphotons, but currently, all of these biphotons have linewidths that are larger than 1 MHz. The other two groups generated the biphotons with the SFWM in cold atoms. In Refs. [44, 45], their biphotons had linewidths of 430 and 380 kHz, and the generation rates per linewidth were about 470 and 540 pairs/(s·MHz),

respectively. It is necessary to switch off the mechanism for cooling and trapping the atoms during biphoton generation, and the duty cycle of the generation was 10%. The above quoted generation rates are averaged over a cycle.

As compared with the biphotons that were generated by the cavity-assisted SPDC in nonlinear crystals or by the SFWM in cold atomic vapors, the biphotons that were previously generated by the SFWM in hot atomic vapors had a broader linewidth and a lower generation rate per linewidth at a given signal-to-background ratio (SBR). The biphotons of hot-atom SFWM in Refs. [10, 57–61] all had linewidths of larger than 1 MHz. In those studies, the pump and coupling fields counter-propagated, and their propagation directions and the single photons' emission directions had a small separation angle. The counter-propagation scheme was commonly used in the experiments of cold atoms, and did not cause problems since the Doppler effect is negligible and the size of cold atomic clouds is normally small. However, this scheme degrades the linewidth and the spectral brightness (i.e., the generation rate per linewidth per pump power) of biphotons in the experiments of hot atoms. In Refs. [10, 57–61], the best spectral brightness is about 230 pairs/(s·mW·MHz) [57].

We generated biphotons with a tunable temporal width from a ^{87}Rb atomic vapor cell by using the SFWM process. The cell was heated to 38°C in the experiment. We employed the all-copropagating scheme, instead of the scheme that was commonly used in the previous studies of SFWM with either cold or hot atomic vapors. In the all-copropagating scheme, the pump and coupling fields propagate in the same direction, and completely overlap the emission directions of the Stokes and anti-Stokes photons. The copropagation configuration maintains a good phase-match condition in the SFWM process. The zero angle separation between the strong driving fields and the single photons enables a low decoherence rate in the Doppler-broadened media. Hence, the best spectral brightness in this study reaches 3,000 pairs/(s·mW·MHz), which is significantly higher than those in the previous studies of the hot-atom SFWM.

In this work, the longest temporal width of the biphoton wave packet is 550 ± 40 ns, which corresponds to a linewidth of 290 ± 20 kHz. To our knowledge, this is the narrowest linewidth to date among all the different kinds of single-mode biphotons. The maximum two-photon correlation function, $g_{as,s}^{(2)}$, or peak SBR of the 290-kHz biphoton wave packet was 5.4, which violates the Cauchy-Schwartz inequality for classical light by 7.3 folds and clearly demonstrates its nonclassicality. As we tune the temporal width of the biphotons to

260 ns, i.e., the linewidth of 610 kHz, their peak SBR is significantly enhanced to 42, which violates the Cauchy-Schwartz inequality by 440 folds and demonstrates that the heralded single photons have a rather high purity. The 610-kHz biphotons have the generation rate per linewidth of 1,500 pairs/(s·MHz), which is the best result among all of the sub-MHz biphoton sources in the literature [34, 38, 44, 45]. The biphoton source of hot-atom SFWM not only has the merit of a linewidth tunable for more than an order of magnitude, but also is capable to set to any frequency in a continuous range of 0.6 GHz or larger. Such temporally-long, high-purity, and spectrally-bright biphotons will be very useful in the application of long-distance quantum communication.

II. EXPERIMENTAL SETUP

Biphotons or a pair of single photons in the experiment were produced from a paraffin-coated glass cell filled with the vapor of isotopically enriched ^{87}Rb atoms. The cylindrical cell has the diameter of 25 mm and is 75 mm long. We heated the cell to 38 °C to maintain the vapor pressure of about 10^{-6} torr or, equivalently, the atomic density of $3.1 \times 10^{10} \text{ cm}^{-3}$. Figure 1 shows the relevant energy levels and transitions of SFWM process for the generation of biphotons. Nearly all population was optically pumped to the ground state of $|5S_{1/2}, F = 2\rangle$. The pump field was red-detuned 2.0 GHz from the transition of $|5S_{1/2}, F = 2\rangle \rightarrow |5P_{3/2}, F'' = 1\rangle$, and the coupling field drove the transition of $|5S_{1/2}, F = 1\rangle \rightarrow |5P_{1/2}, F' = 2\rangle$ resonantly. Due to the vacuum fluctuation, a pair of anti-Stokes and Stokes photons can be spontaneously emitted. The frequencies of the pump field, anti-Stokes photon, coupling field, and Stokes photon form the resonant four-photon transition. The hyperfine optical pumping (HOP) field is not a part of the SFWM process, and was employed to empty the population in $|5S_{1/2}, F = 1\rangle$.

The coupling field came from a 795-nm external-cavity diode laser (ECDL) of Toptica DL DLC pro 795. We stabilized the coupling frequency with the saturated absorption spectroscopy, and the frequency fluctuation was about ± 0.3 MHz. The pump field originated from a homemade 780-nm ECDL. We stabilized the pump frequency with a wavelength meter (HighFinesse WSU-30), and the frequency fluctuation was about ± 1.5 MHz. The HOP field came from a laser amplifier (Toptica Boos TA). We seeded the amplifier with the light from a homemade 780-nm bare-diode laser, which was injection-locked by the pump laser light

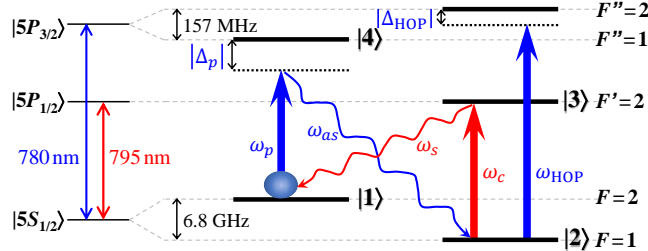


FIG. 1: Relevant energy levels of ^{87}Rb atoms and the transition diagram. In the SFWM scheme, ω_p , ω_{as} , ω_c , and ω_s represent the frequencies of the pump field, anti-Stokes photon, coupling field, and Stokes photon, forming the four-photon resonance condition. The detuning of the pump field, Δ_p , is about -2.0 GHz. The frequency of the hyperfine optical pumping (HOP) field is denoted by ω_{HOP} , and has the detuning, Δ_{HOP} , of -80 MHz.

with the offset frequency provided by an electro-optic modulator (EOM). The HOP field was red-detuned 80 MHz from the transition of $|5S_{1/2}, F = 1\rangle \rightarrow |5P_{3/2}, F'' = 2\rangle$, and had the same frequency fluctuation as the pump laser.

The experimental setup is shown in Fig. 2. Both of the pump and coupling fields were linearly polarized in the orthogonal configuration, i.e., they had the p and s polarizations, respectively. We completely overlapped the two fields with a polarization beam splitter. Before the vapor cell, the 780-nm and 795-nm bandpass filters were installed for the pump and coupling fields. These filters together with the 795-nm and 780-nm bandpass filters after the vapor cell prevented the strong pump and coupling light from entering the Stokes and anti-Stokes single-photon counting modules (SPCMs), respectively. The dichroic mirror right after the cell separated the 780-nm and 795-nm light. After the dichroic mirror, the combination of the quarter-wave plate, half-wave plate, and Glan-Thompson polarizer attenuated the pump (or coupling) light by 60 dB (or 48 dB), and allowed a high transmission of the s -polarized anti-Stokes photons (or p -polarized Stokes photons). A set of two etalons in series further reduced the pump (or coupling) light by about 74 dB (or 88 dB). Considering the above attenuation factors, we estimate that the pump (or coupling) light of 1 mW contributed merely about 100 (or 64) counts/s the anti-Stokes (or Stokes) SPCM. The two SPCMs (Excelitas SPCM-AQRH-13-FC) have the dark-count rates of 140 ± 5 and 220 ± 20 counts/s.

Each set of the two etalons has the linewidth of about 35 MHz, and provides a peak

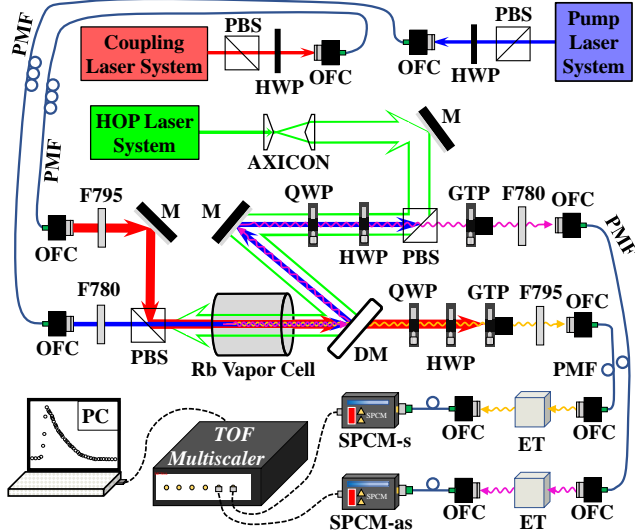


FIG. 2: Experimental setup. Blue, red, and green lines represent the laser beams of the pump, coupling, and HOP fields. Violet and orange wiggly lines indicate the optical paths of the anti-Stokes and Stokes photons. PBS: polarizing beam splitter, HWP: half-wave plate, OFC: optical fiber coupler, PMF: polarization-maintained optical fiber, F780 (F795): a set of three 780 nm (795 nm) bandpass filters in series, M: mirror, QWP: quarter-wave plate, GTP: Glan-Thompson polarizer, DM: dichroic mirror, ET: a set of two etalons in series, and SPCM-as (SPCM-s): single-photon counting module for anti-Stokes (Stokes) photons.

transmission of around 37% (or 42%) for the anti-Stokes (or Stokes) photons. Because of the high extinction ratios of the etalons, we were able to make the coupling field, Stokes photons, pump field, and anti-Stokes photons propagate in the same direction and completely overlap inside the vapor cell. The anti-Stokes photon propagates with the light speed in vacuum, because of the large one-photon detuning in the Raman process of the pump field and anti-Stokes photon. The Stokes photon is slow light due to the effect of electromagnetically induced transparency (EIT) in the Raman process of the coupling field and Stokes photon. Thus, the anti-Stokes SPCM detected a photon first, triggering the TOF multiscalar, and after some delay time the Stokes SPCM detected another, recorded as a coincidence count. The overall collection efficiencies, including the SPCMs' quantum efficiencies, of the anti-Stokes and Stokes photons were 8.4% and 13%, respectively.

The pump and coupling fields co-propagated inside the vapor cell, and had the e^{-2} full widths of 1.4 and 1.5 mm, respectively. According to the beam width and power, we esti-

mated that the peak intensity of a 0.5-mW pump beam corresponds to the Rabi frequency of 2.0Γ , where $\Gamma = 2\pi \times 6$ MHz is the spontaneous decay rate of the excited states. Under the similar estimation, the peak intensity of a 1-mW coupling beam corresponds to the Rabi frequency of 2.9Γ . The *s*-polarization HOP field has a donut-shaped beam profile with the inner and outer e^{-2} diameters of about 8.5 and 11.5 mm. It propagated in the direction opposite to the pump and coupling's propagation direction. We kept the power of the HOP at 18 mW throughout the experiment. The ratio of the average intensity in the donut area to that in the region of biphoton generation was approximately 30, and the peak Rabi frequency in the donut area is 3.4Γ .

To study the experimental condition, we measured the EIT spectrum. An input probe field was employed in the measurement. This probe field came from a homemade 795-nm bare-diode laser, which was injection-locked by the coupling laser light with the offset frequency provided by an EOM. We swept the probe frequency across the Stokes transition by tuning the driving frequency of the EOM around 6.835 GHz, i.e., the frequency difference between the two hyperfine levels of the ground state $|5S_{1/2}\rangle$. Because of the injection-lock scheme, fluctuation of the frequency difference between the probe and coupling fields is completely negligible. The input probe field had the e^{-2} full widths of 0.6 mm, and its power was 50 nW. This field is weak enough that it can be treated as the perturbation in the system. We experimentally verified that the probe transmission of the EIT spectrum did not change as the probe power was increased by more than two folds. The input probe field was blocked during the biphoton generation.

III. THEORETICAL PREDICITONS

We utilized the time correlation function between the anti-Stokes and Stokes photons, i.e., the biphoton wave packet, to make theoretical predictions, and compared the experimental data with the predictions. The two-photon time correlation is shown below [11].

$$G^{(2)}(\tau) = \left| \int_{-\infty}^{\infty} d\delta \frac{1}{2\pi} e^{-i\delta\tau} \int_{-\infty}^{\infty} d\omega_D \frac{1}{\sqrt{\pi}\Gamma_D} e^{-\omega_D^2/\Gamma_D^2} \frac{\sqrt{k_{as}k_s}L}{2} \chi(\delta, \omega_D) \right. \\ \left. \times \text{sinc}\left[\frac{k_s L}{4}\xi(\delta, \omega_D)\right] e^{i(k_s L/4)\xi(\delta, \omega_D)} \right|^2, \quad (1)$$

where τ is the delay time of the Stokes photon, δ is the two-photon detuning of the Raman transition between the anti-Stokes photon and pump field (or $-\delta$ is that between the Stokes

photon and coupling field), ω_D is the Doppler shift, Γ_D is the Doppler width, k_{as} and k_s are the wave vectors of the two photons, L is the medium length, $\chi(\delta, \omega_D)$ is the cross-susceptibility of the Stokes photon induced by the anti-Stokes photon, and $\xi(\delta, \omega_D)$ is the self-susceptibility of the Stokes photon. The formulas relating the cross-susceptibility and self-susceptibility to the experimental parameters are given by

$$\frac{\sqrt{k_{as}k_s}L}{2}\chi(\delta, \omega_D) = \frac{\sqrt{\alpha_{as}\alpha_s}\sqrt{\Gamma_3\Gamma_4}}{4} \frac{\Omega_p}{\Delta_p - \omega_D + i\Gamma_4/2} \frac{\Omega_c}{\Omega_c^2 - 4(\delta + i\gamma)(\delta + \omega_D + i\Gamma_3/2)}, \quad (2)$$

$$\frac{k_sL}{4}\xi(\delta, \omega_D) = \frac{\alpha_s\Gamma_3}{2} \frac{\delta + i\gamma}{\Omega_c^2 - 4(\delta + i\gamma)(\delta + \omega_D + i\Gamma_3/2)}, \quad (3)$$

where $\alpha_s = n\sigma_s L$ (n is the atomic density and σ_s is the resonant absorption cross section of the Stokes transition) represents the optical depth of the entire atoms interacting with the Stokes photon resonantly, α_{as} means the similar optical depth of the anti-Stokes transition, Ω_p and Ω_c are the Rabi frequencies of the pump and coupling fields, Γ_3 and Γ_4 are the spontaneous decay rates of the excited states (i.e., $|3\rangle$ and $|4\rangle$ in Fig. 1) in the Stokes and anti-Stokes transitions, respectively, Δ_p is the detuning of the pump field, and γ is the dephasing rate of the ground-state coherence, i.e., the decoherence rate. Since the difference between Γ_3 and Γ_4 is merely about 5% in our case, we neglect the difference and set $\Gamma_3 = \Gamma_4 \equiv \Gamma = 2\pi \times 6$ MHz in this work. Due to the temperature of the vapor cell being 38°C, $\Gamma_D = 54\Gamma$ in the calculation.

We measured the EIT spectrum to characterize the experimental parameters [62, 63]. The theoretical EIT spectrum is given by the self-susceptibility $k_sL\xi(\delta, \omega_D)$ of the Stokes photon or, equivalently, the classical probe field. Considering a Doppler-broadened medium, the imaginary part of $k_sL\xi(\delta, \omega_D)$ is integrated over all the velocity groups. Thus, we obtain the transmission, T , of the probe field as the following:

$$T = \exp \left\{ - \int_{-\infty}^{\infty} d\omega_D \frac{1}{\sqrt{\pi\Gamma_D}} e^{-\omega_D^2/\Gamma_D^2} \text{Im}[k_sL\xi(\delta, \omega_D)] \right\}. \quad (4)$$

In the experiment, we fitted the measured EIT spectra with the calculation results of the above formula. The best fits determine the experimental parameters of α_s , Ω_c , and γ .

IV. RESULTS AND DISCUSSION

Once the biphoton is generated, the anti-Stokes photon with the light speed in vacuum quickly exits the medium, and the Stokes photon is the slow light and propagates in the

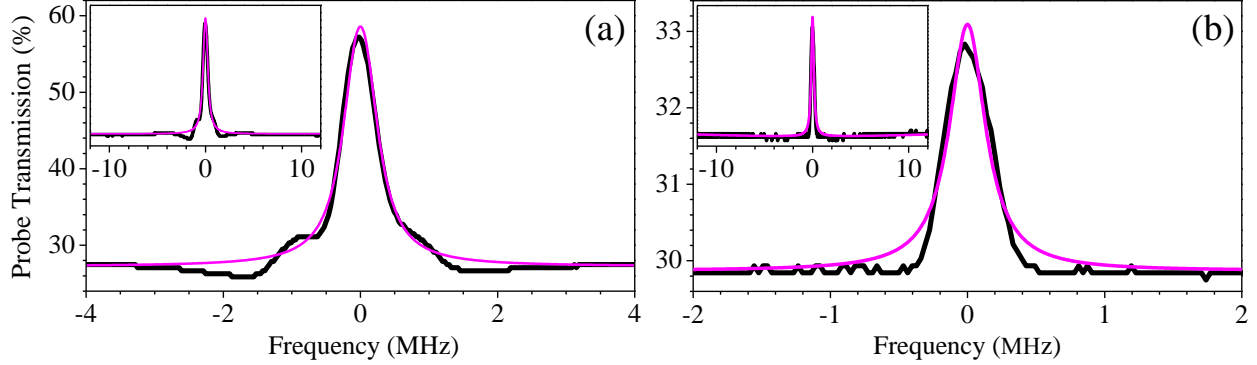


FIG. 3: Representative EIT spectra of the probe field. The powers of the coupling field are 1 mW in (a) and 0.05 mW in (b), that of the HOP field is 18 mW, and that of the input probe field is 50 nW. The pump field had no effect on the spectra. Insets show the same spectra with a larger frequency range. Black lines are the experimental data. Magenta lines represent the best fits of the numerical result calculated with Eq. (4). The best fits determine the FWHMs of 560 kHz in (a) and 300 kHz in (b). The values of OD, coupling Rabi frequency, and decoherence rate are 80, 2.6Γ , and 0.028Γ in (a), and 82, 0.65Γ , and 0.024Γ in (b).

medium under the presence of the coupling and pump fields. Since the pump field was far detuned, it had a negligible effect on the Stokes photon. The temporal profile of the probability of detecting the Stokes photon, i.e., the biphoton wave packet, is mainly determined by the EIT effect. Consequently, the measured EIT spectrum can reveal the experimental condition of optical depth (α_s), coupling Rabi frequency (Ω_c), and decoherence rate (γ) for the theoretical calculation to predict the biphoton wave packet. We measured the spectra with an input probe field under the presence of the coupling, HOP, and pump fields. The input probe field is weak enough that it can be treated as the perturbation in the system. The coupling power was varied and set to either 0.02, 0.05, 0.1, 0.2, 0.5, 1, 2, or 5 mW. Since we intended to make the experimental condition as close to the biphoton generation as possible, the HOP and pump fields were also present in the spectrum measurement. Nevertheless, at each coupling power the spectra with and without the pump field had no difference. The black lines in Figs. 3(a) and 3(b) are the representative EIT spectra at the coupling powers of 1 and 0.05 mW.

We fitted the EIT spectra of different coupling powers with the numerical result calculated from Eq. (4). The value of α_s is uniquely determined by the baseline transmission of the

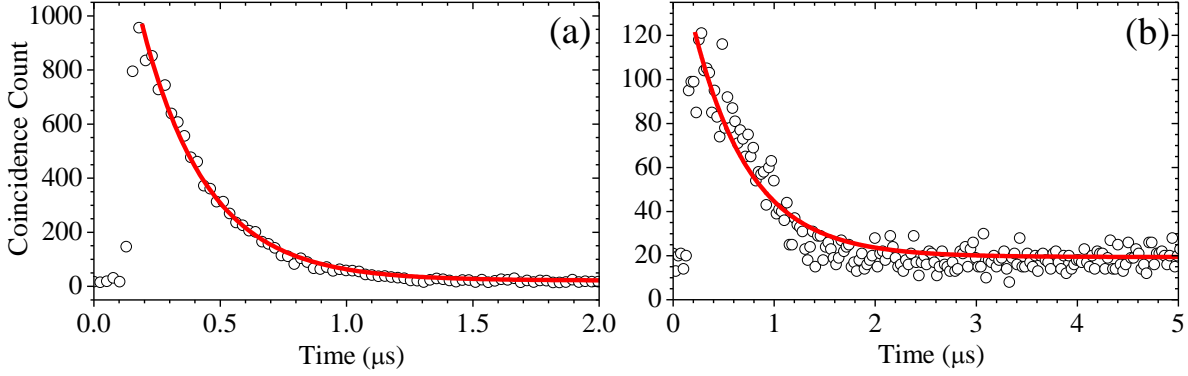


FIG. 4: Representative data of biphoton wave packets measured at the coupling power of 1 mW in (a) and 0.05 mW in (b). The pump and HOP powers are 0.5 mW and 18 mW. Circles are the two-photon coincidence counts and red lines are the best fits of the exponential-decay function. The e^{-1} time constants of the best fits are 260 ns in (a) and 560 ns in (b), corresponding to the linewidths of 610 kHz and 280 kHz, respectively. We determine the peak signal-to-background ratios of 42 in (a) and 5.4 in (b).

spectrum. At a given α_s , the peak transmission and width of the EIT window resolve the values of Ω_c and γ . Thus, the values of α_s , Ω_c , and γ are unambiguously determined by the best fits of the EIT spectra. The magenta lines in Figs. 3(a) and 3(b) are the best fits. In Fig. 3(a), the experimental spectrum shows small peaks and dips on the two sides of the central EIT peak, which are not present in the best fit calculated from Eq. (4). These minor peaks and dips were caused by the residual light of the HOP field in its hollow region. As we turned off the HOP field, they disappeared. In Fig. 3(b), the part of the experimental spectrum near the baseline deviates from the best fit. This deviation was also caused by the HOP field.

We systematically measured the biphoton data at different coupling powers of 0.02, 0.05, 0.1, 0.2, 0.5, 1, 2, and 5 mW. The circles in Figs. 4(a) and 4(b) are the representative biphoton wave packets, i.e., the coincidence count as a function of the delay time between the Stokes and anti-Stokes photons, taken at the coupling powers of 1 and 0.05 mW. The bin time of data points is 25.6 ns. At the coupling power of 0.05 mW, the pump power was optimized for the best signal-to-background ratio (SBR), and the HOP power was optimized for the longest temporal width without degrading the SBR. We used the same pump and HOP powers for all the biphoton measurements. Since the pump power was kept the same

in the biphoton generation, the detection rates (excluding the SPCM's dark counts) of the anti-Stokes photons at different coupling powers were all around 840 ± 50 counts/s. The fluctuation of $\pm 6\%$ was mainly comes from the variation of the collection efficiency of anti-Stokes photons caused by the drift of the etalon's temperature.

The EIT spectral profile of a Doppler-broadened medium can be approximated as a Lorentzian function according to our study, which will be published elsewhere. Thus, the biphoton wave packet should behave like or close to an exponential-decay function, i.e., $y(x) = y_0 + S \exp[-(x - x_0)/\tau]$. This is indeed the case for all the observed biphoton data. We resolved y_0 from the data first, set x_0 to 200 ns, and then fitted the data with the fitting parameters of S and τ . The red lines in Figs. 4(a) and 4(b) are the best fits. In each biphoton wave packet, we determine the linewidth from $\tau^{-1}/(2\pi)$ of the best fit and calculate the SBR from the ratio of S to y_0 .

To study the relation between the temporal width of the biphoton wave packet and the linewidth of the corresponding EIT spectrum, we plot the biphoton time constant (τ) and the reciprocal of the EIT FWHM (Γ_{EIT}^{-1}) as functions of the coupling power in Fig. 5. Although there exist some discrepancies between the two data sets, their overall behaviors are very similar. A smaller coupling power results in a longer temporal width of the biphoton wave packet or a narrower linewidth of the EIT spectrum. Furthermore, the biphoton's temporal width (or EIT linewidth) asymptotically approaches an upper (or lower) limit, which is theoretically equal to $(2\gamma)^{-1}$. The temporal width (or linewidth) of the biphoton wave packet is limited to 550 ± 40 ns (or 290 ± 20 kHz) measured at the coupling power of 0.05 mW or less. Using the value of γ determined from the corresponding EIT spectrum, $(2\gamma)^{-1} \approx 530$ ns (or $\gamma/\pi \approx 300$ kHz). The linewidth of EIT spectrum measured with classical light can be a good indicator of the temporal width or spectral linewidth of biphoton wave packet.

We further employed Eq. (1) to predict the biphoton wave packet of each coupling power, and compared the experimental data with the theoretical predictions. In the numerical calculation of Eq. (1), the parameters of the OD (α_s), coupling Rabi frequency (Ω_c), and decoherence rate (γ) were set under the following consideration. As mentioned earlier, the best fit of the EIT spectrum measured at each coupling power had determined a set of α_s , Ω_c , and γ . First of all, we fitted the data points of Ω_c^2 versus the coupling power, P_c , with a straight line of zero interception. The best fit gives the relation of $\Omega_c = 2.7\Gamma\sqrt{P_c}/(1 \text{ mW})$. Secondly, the best-fit value of γ slightly increased with the coupling power (see the examples

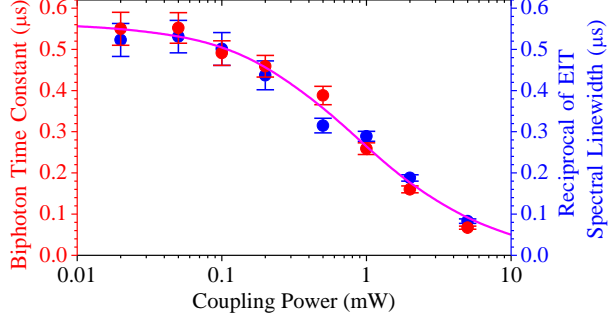


FIG. 5: Time constant of the biphoton wave packet (red) and the reciprocal of FWHM of the EIT spectrum (blue) as functions of the coupling power. Red and blue circles are the experimental data. Magenta line is the theoretical prediction calculated with $\alpha_s = 82$, $\gamma = 0.025\Gamma$, and $\Omega_c = 2.7\Gamma\sqrt{P_c/(1 \text{ mW})}$ where P_c is the coupling power.

in Fig. 3). The biphoton's temporal width of a small coupling power is sensitive to γ , but that of a large coupling power is not. Hence, we chose the average value of γ 's of the three smallest coupling powers in the calculation. Finally, the values of α_s determined from the experimental spectra vary from 79 to 84, and the variation affects the prediction little. We set α_s to the intermediate value, i.e., 82. The other parameters of the pump Rabi frequency (Ω_p), pump detuning (Δ_p), and anti-Stokes photon's OD (α_{as}) do not affect the shape and width of the biphoton wave packet, and only change its overall magnitude. In Fig. 5, the magenta line is the theoretical prediction calculated with $\alpha_s = 82$, $\gamma = 0.025\Gamma$, and $\Omega_c = 2.7\Gamma\sqrt{P_c/(1 \text{ mW})}$. The consistency between the experimental data and theoretical predictions is satisfactory.

The generation rate is an important figure of merit of a biphoton source. We show how the coupling power or equivalently Ω_c^2 affects the biphoton generation rate in Fig. 6(a). The black circles are the experimental data which are the results of the coincidence count per second or the detection rate divided by the product of the collection efficiencies of the anti-Stokes and Stokes photons. As Ω_c^2 increases, the generation rate is enhanced accordingly, but eventually gets saturation. The observation is in agreement with the situation that the Stokes photon propagates in the EIT medium like slow light and a larger Ω_c^2 makes the transmission higher. At a very large Ω_c^2 , all the generated Stokes photons can move out of the medium with a little attenuation and the generation rate saturates. To simulate the generation rate as a function of the coupling power, the same predictions of the biphoton wave packet in Fig. 5

were used. The area below the wave packet is proportional to the generation rate. We multiplied the area by a normalization factor to obtain the predictions of generation rate as shown by the magenta line in Fig. 6(a). The normalization factor minimizes the standard deviation between the experimental data and the predictions. Other than getting saturation a little faster, the experimental data behave similarly to the theoretical predictions.

The spectral brightness is defined as the generation rate per pump power per spectral linewidth. We plot the spectral brightness as a function of the coupling power in Fig. 6(b). The circles are the experimental data. The magenta line represents the theoretical predictions which are the predictions in Fig. 6(a) divided by the product of the prediction in Fig. 5 and the pump power of 0.5 mW. At the coupling power of 1 mW, the biphoton source reaches the maximum spectral brightness of 3,000 pairs/(s·mW·MHz). As the coupling power gets larger than 1 mW, the generation rate becomes saturated and increases a little, but the linewidth still increases prominently. The maximum of the spectral brightness locating around 1 mW is expected.

The SBR in the biphoton wave packet can provide the information of the two-photon correlation function $g_{as,s}^{(2)}$ between the anti-Stokes and Stokes photons. Since the biphoton wave packet is an exponential-decay function, the SBR ($= S/y_0$ mention earlier) is equal to the maximum $g_{as,s}^{(2)}$. Figure 6(c) shows the SBR as a function of the coupling power. The black circles are the experimental data, and the magenta lines represent the theoretical predictions. To make the predictions of SBR, we utilized Eq. (1) to calculate the biphoton wave packets with the same parameters as those in Fig. 5. The effect of the rise time of 35 ns observed in the experimental data is also included in the calculation. Next, we got the ratio of the peak of the theoretical waveform to the background count rate. This background count rate, B , was measured regardless of the anti-Stokes photons, and relates to the coupling power, P_c , as $B = 240 + 320[P_c/(1 \text{ mW})]^{0.53}$ counts/s. Finally, we multiplied the above ratio by a normalization factor to obtain the predicted SBR. In Fig. 6(c), the behavior of the experimental data agrees with that of the theoretical predictions.

In this work, the maximum $g_{as,s}^{(2)}$ of the biphotons of the narrowest linewidth, measured at the coupling power of 0.05 mW, is 5.4. The result violates the Cauchy-Schwartz inequality for classical light, i.e., $[g_{as,s}^{(2)}]^2/[g_{as,as}^{(2)} \cdot g_{s,s}^{(2)}] \leq 1$, by 7 folds, and clearly demonstrates nonclassicality of these 290-kHz biphotons. As we set the coupling power to 2 mW, the biphotons had the temporal width of 160 ns, i.e., the linewidth of just below 1 MHz. The SBR of these

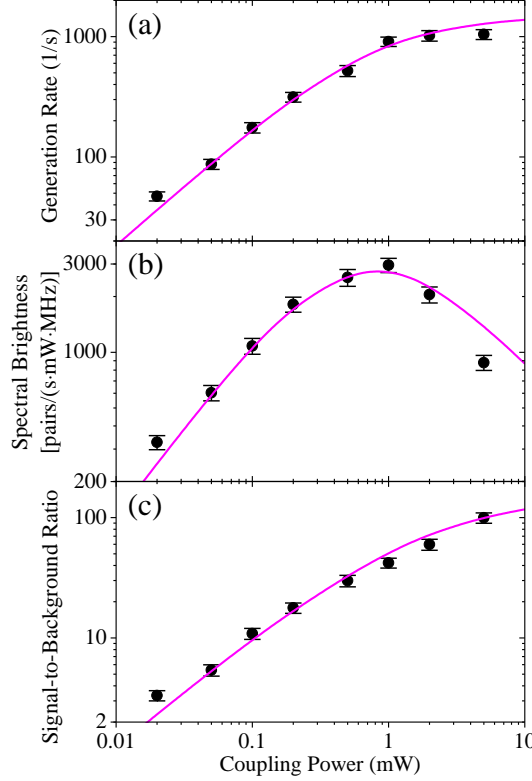


FIG. 6: The generation rate, spectral brightness, and peak signal-to-background ratio of biphotons as functions of the coupling power in (a), (b), and (c), respectively. Black circles are the experimental data. Magenta lines are the theoretical predictions calculated with the same parameters as those in Fig. 5.

1-MHz biphotons was significantly enhanced to 60 which violates the Cauchy-Schwartz inequality by 900 folds, exhibiting high purity. At the coupling power of 1 mW and the pump power of 0.5 mW, the 610-kHz biphoton source had the SBR of 42 and the generation rate per linewidth of 1,500 pairs/(s·MHz). By changing the pump power from 0.5 to 8 mW, we were able to enhance the generation rate per linewidth of the biphoton source to 2.3×10^4 pairs/(s·MHz) at expense of the SBR being reduced to 6.7 and the linewidth being slightly increased to 670 kHz.

V. PROSPECTS AND CONCLUSION

We have generated biphotons from the ^{87}Rb atomic vapor cell by using the SFWM process, and systematically studied the temporal width or spectral linewidth, the generation

rate, the spectral brightness, and the maximum two-photon correlation function $g_{as,s}^{(2)}$ or SBR as functions of the coupling power or equivalently Ω_c^2 . The coupling power was varied from 0.02 to 5 mW. The consistency between the experimental data and theoretical predictions that were calculated from Eq. (1) is satisfactory.

Here, we employed the all-copropagating scheme. The scheme not only maintains a good phase-match condition in the SFWM, but also enables a low decoherence rate in the Doppler-broadened medium. Consequently, we have been able to generate sub-MHz biphotons, which could previously not be achieved with hot atom vapors. In addition, the spectral brightness of our sub-MHz biphoton source is significantly higher than those of the early hot-atom SFWM studies. Please note that a longer vapor cell can have a larger OD, resulting in a higher biphoton generation rate. However, the OD-enhancement effect is cancelled out by a larger phase mismatch in the counter-propagation scheme due to a longer optical path. The all-copropagating scheme demonstrated here can maintain a good phase-match condition regardless of the length of the vapor cell. Thus, one can use a longer cell to achieve a higher generation rate or spectral brightness. The results of the generation rate and spectral brightness presented here can be scaled up with the square of the OD or cell length.

The linewidth-tunable biphotons produced here can compete with those generated by the cavity-assisted SPDC and by the cold-atom SFWM. We were able to tune the linewidth down to 290 ± 20 kHz. Previously, the single-mode biphoton sources of cavity-assisted SPDC all had linewidths of larger than 1 MHz [8], and those of cold-atom SFWM had the narrowest linewidth of 380 kHz [45]. The multi-mode biphoton sources can have a frequency mode span of a few hundred MHz, and the linewidth of a mode can be as narrow as 265 kHz [38]. In the literature, two multi-mode biphoton sources of cavity-assisted SPDC and two single-mode ones of cold-atom SFWM achieved the sub-MHz linewidth, and their generation rates per linewidth were 88, 324, 470, and 540 pairs/(s·MHz) [34, 38, 44, 45]. Our biphoton source of 610-kHz linewidth had a generation rate per linewidth of 1,500 pairs/(s·MHz) at an SBR of 42. As we increased the pump power by 16 folds, the SBR became 6.7 and the generation rate per linewidth was enhanced to 2.3×10^4 pairs/(s·MHz).

In conclusion, biphotons are pairs of time-energy entangled single photons and can be employed as heralded photonic qubits in long-distance quantum communication. The biphoton source of hot-atom SFWM not only has the merit of a linewidth tunable for more than an

order of magnitude, but also is capable to set to any frequency in a continuous range of 0.6 GHz or larger. Since the sub-MHz, high-purity, and spectrally-bright biphotons produced in this work will be the versatile and powerful carriers of information, the results of this work have become an important milestone in the quantum technology utilizing photonic qubits.

Acknowledgments

This work was supported by Grant Nos. 108-2639-M-007-001-ASP and 109-2639-M-007-001-ASP of the Ministry of Science and Technology, Taiwan.

- [1] L. M. Duan, M. D. Lukin, J. I. Cirac, and P. Zoller, “Long-distance quantum communication with atomic ensembles and linear optics,” *Nature* **414**, 413-418 (2001).
- [2] N. Gisin, G. Ribordy, W. Tittel, and H. Zbinden, “Quantum cryptography,” *Rev. Mod. Phys.* **74**, 145-195 (2002).
- [3] R. H. Hadfield, “Single-photon detectors for optical quantum information applications,” *Nat. Photon.* **3**, 696-705 (2009).
- [4] N. Sangouard, C. Simon, H. de Riedmatten, and N. Gisin, “Quantum repeaters based on atomic ensembles and linear optics,” *Rev. Mod. Phys.* **83**, 33-80 (2011).
- [5] Q.-C. Sun, Y.-F. Jiang, Y.-L. Mao, L.-X. You, W. Zhang, W.-J. Zhang, X. Jiang, T.-Y. Chen, H. Li, Y.-D. Huang, X.-F. Chen, Z. Wang, J. Fan, Q. Zhang, and J.-W. Pan, “Entanglement swapping over 100 km optical fiber with independent entangled photon-pair sources,” *Optica* **4**, 1214-1218 (2017).
- [6] R. Ghosh and L. Mandel, “Observation of Nonclassical Effects in the Interference of Two Photons,” *Phys. Rev. Lett.* **59** 1903-1905 (1987).
- [7] L. Mandel, “Quantum effects in one-photon and two-photon interference,” *Rev. Mod. Phys.* **71**, S274-S282 (1999).
- [8] O. Slattery, L. Ma, K. Zong, and X. Tang, “Background and review of cavity-enhanced spontaneous parametric down-conversion,” *J. Resv. Natl. Inst. Stan.* **124**, 124019 (2019).
- [9] V. Balić, D. A. Braje, P. Kolchin, G. Y. Yin, and S. E. Harris, “Generation of Paired Photons with Controllable Waveforms,” *Phys. Rev. Lett.* **94**, 183601 (2005).

[10] C. Shu, P. Chen, T. K. A. Chow, L. Zhu, Y. Xiao, M. M. T. Loy, and S. Du, “Subnatural-linewidth biphotons from a Doppler-broadened hot atomic vapour cell,” *Nat. Commun.* **7**, 12783 (2016).

[11] S. Du, J. Wen, and M. H. Rubin, “Narrowband biphoton generation near atomic resonance,” *J. Opt. Soc. Am. B* **25**, C98-C108 (2008).

[12] M. P. Hedges, J. J. Longdell, Y. Li, and M. J. Sellars, “Efficient quantum memory for light,” *Nature (London)* **465**, 1052-1056 (2010).

[13] Y.-H. Chen, M.-J. Lee, I.-C. Wang, S. Du, Y.-F. Chen, Y.-C. Chen, and I. A. Yu, “Coherent Optical Memory with High Storage Efficiency and Large Fractional Delay,” *Phys. Rev. Lett.* **110**, 083601 (2013).

[14] D. Schraft, M. Hain, N. Lorenz, and T. Halfmann, “Stopped Light at High Storage Efficiency in a $\text{Pr}^{3+}:\text{Y}_2\text{SiO}_5$ Crystal,” *Phys. Rev. Lett.* **116**, 073602 (2016).

[15] Y.-W. Cho, T. Campbell, J. L. Everett, J. Bernu, D. B. Higginbottom, M. T. Cao, J. Geng, N. P. Robins, P. K. Lam, and B. C. Buchler, “Highly efficient optical quantum memory with long coherence time in cold atoms,” *Optica* **3**, 100-107 (2016).

[16] P. Vernaz-Gris, K. Huang, M. Cao, A. S. Sheremet, and J. Laurat, “Highly-efficient quantum memory for polarization qubits in a spatially-multiplexed cold atomic ensemble,” *Nat. Commun.* **9**, 363 (2018).

[17] Y.-F. Hsiao, P.-J. Tsai, H.-S. Chen, S.-X. Lin, C.-C. Hung, C.-H. Lee, Y.-H. Chen, Y.-F. Chen, I. A. Yu, and Y.-C. Chen, “Highly Efficient Coherent Optical Memory Based on Electromagnetically Induced Transparency,” *Phys. Rev. Lett.* **120**, 183602 (2018).

[18] Y. Wang, J. Li, S. Zhang, K. Su, Y. Zhou, K. Liao, S. Du, H. Yan, and S.-L. Zhu, “Efficient quantum memory for single-photon polarization qubits,” *Nat. Photon.* **13**, 346-351 (2019).

[19] P.-J. Tsai, Y.-F. Hsiao, and Y.-C. Chen, “Quantum storage and manipulation of heralded single photons in atomic memories based on electromagnetically induced transparency,” *Phys. Rev. Research* **2**, 033155 (2020).

[20] A. G. Radnaev, Y. O. Dudin, R. Zhao, H. H. Jen, S. D. Jenkins, A. Kuzmich and T. A. B. Kennedy, “A quantum memory with telecom-wavelength conversion,” *Nat. Phys.* **6**, 894-899 (2010).

[21] A. Feizpour, M. Hallaji, G. Dmochowski, and A. M. Steinberg, “Observation of the nonlinear phase shift due to single post-selected photons,” *Nat. Phys.* **11**, 905-909 (2015).

- [22] K. M. Beck, M. Hosseini, Y. Duan, and V. Vuletić, “Large conditional single-photon cross-phase modulation,” *Proc. Natl. Acad. Sci. U.S.A.* **113**, 9740-9744 (2016).
- [23] D. Tiarks, S. Schmidt, G. Rempe, and S. Dürr, “Optical π phase shift created with a single-photon pulse,” *Science Adv.* **2**, e1600036 (2016).
- [24] B. Hacker, S. Welte, G. Rempe, and S. Ritter, “A photon-photon quantum gate based on a single atom in an optical resonator,” *Nature (London)* **536**, 193-196 (2016).
- [25] J. S. Neergaard-Nielsen, B. M. Nielsen, H. Takahashi, A. I. Vistnes, and E. S. Polzik, “High purity bright single photon source,” *Opt. Express* **15**, 7940-7949 (2007).
- [26] X.-H. Bao, Y. Qian, J. Yang, H. Zhang, Z.-B. Chen, T. Yang, and J.-W. Pan, “Generation of narrow-band polarization-entangled photon pairs for atomic quantum memories,” *Phys. Rev. Lett.* **101**, 190501 (2008).
- [27] F. Wolfgramm, X. Xing, A. Cerè, A. Predojević, A. M. Steinberg, and M. W. Mitchell, “Bright filter-free source of indistinguishable photon pairs,” *Opt. Express* **16**, 18145-18151 (2008).
- [28] M. Scholza, L. Koch, R. Ullmann, and O. Benson, “Single-mode operation of a high-brightness narrow-band single-photon source,” *Appl. Phys. Lett.* **94**, 201105 (2009).
- [29] C.-S. Chuu, G. Y. Yin, and S. E. Harris, “A miniature ultrabright source of temporally long, narrowband biphotons,” *Appl. Phys. Lett.* **101**, 051108 (2012).
- [30] J. Fekete, D. Rieländer, M. Cristiani, and H. de Riedmatten, “Ultranarrow-band photon-pair source compatible with solid state quantum memories and telecommunication networks,” *Phys. Rev. Lett.* **110**, 220502 (2013).
- [31] Z.-Y. Zhou, D.-S. Ding, Y. Li, F.-Y. Wang, and B.-S. Shi, “Cavity-enhanced bright photon pairs at telecom wavelengths with a triple-resonance configuration,” *J. Opt. Soc. Am. B* **31**, 128-134 (2014).
- [32] A. Lenhard, M. Bock, C. Becher, S. Kucera, J. Brito, P. Eich, P. Müller, and J. Eschner, “Telecom-heralded single-photon absorption by a single atom,” *Phys. Rev. A* **92**, 063827 (2015).
- [33] D. Rieländer, A. Lenhard, M. Mazzera, and H. de Riedmatten, “Cavity enhanced telecom heralded single photons for spin-wave solid state quantum memories,” *New J. Phys.* **18**, 123013 (2016).
- [34] M. Rambach, A. Nikolova, T. J. Weinhold, and A. G. White, “Sub-megahertz linewidth single photon source,” *APL Photonics* **1**, 096101 (2016).

[35] C.-H. Wu, T.-Y. Wu, Y.-C. Yeh, P.-H. Liu, C.-H. Chang, C.-K. Liu, T. Cheng, and C.-S. Chuu, “Bright single photons for light-matter interaction,” *Phys. Rev. A* **96**, 023811 (2017).

[36] P.-J. Tsai, and Y.-C. Chen, “Ultrabright, narrow-band photon-pair source for atomic quantum memories,” *Quantum Sci. Technol.* **3**, 034005 (2018).

[37] K. Niizeki, K. Ikeda, M. Zheng, X. Xie, K. Okamura, N. Takei, N. Namekata, S. Inoue, H. Kosaka, and T. Horikiri, “Ultrabright narrow-band telecom two-photon source for long-distance quantum communication,” *Appl. Phys. Express* **11**, 042801 (2018).

[38] J. Liu, J. Liu, P. Yu, and G. Zhang, “Sub-megahertz narrow-band photon pairs at 606 nm for solid-state quantum memories,” *APL Photon.* **5**, 066105 (2020).

[39] J. K. Thompson, J. Simon, H. Loh, and V. Vuletić, “A High-Brightness Source of Narrowband, Identical-Photon Pairs,” *Science* **313**, 74-77 (2006).

[40] P. Kolchin, C. Belthangady, S. Du, G. Y. Yin, and S. E. Harris, “Electro-Optic Modulation of Single Photons,” *Phys. Rev. Lett.* **101**, 103601 (2008).

[41] C. Belthangady, S. Du, C.-S. Chuu, G. Y. Yin, and S. E. Harris, “Modulation and measurement of time-energy entangled photons,” *Phys. Rev. A* **80**, 031803 (2009).

[42] S. Yun, J. Wen, P. Xu, M. Xiao, and S.-N. Zhu, “Generation of frequency-correlated narrow-band biphotons from four-wave mixing in cold atoms,” *Phys. Rev. A* **82**, 063830 (2010).

[43] H. Yan , S. Zhang, J. F. Chen, M. M. T. Loy, G. K. L. Wong, and S. Du, “Generation of Narrow-Band Hyperentangled Nondegenerate paired photons,” *Phys. Rev. Lett.* **106**, 033601 (2011).

[44] L. Zhao, X. Guo, C. Liu, Y. Sun, M. M. T. Loy, and S. Du, “Photon pairs with coherence time exceeding 1 μ s,” *Optica* **1**, 84-88 (2014).

[45] Z. Han, P. Qian, L. Zhou, J. F. Chen, and W. Zhang, “Coherence time limit of the biphotons generated in a dense cold atom cloud,” *Sci. Rep.* **5**, 9126 (2015).

[46] L. Zhao, X. Guo, Y. Sun, Y. Su, M. M. T. Loy, and S. Du, “Shaping the Biphoton Temporal Waveform with Spatial Light Modulation,” *Phys. Rev. Lett.* **115**, 193601 (2015).

[47] P. Farrera, G. Heinze, B. Albrecht, M. Ho, M. Chávez, C. Teo, N. Sangouard, and H. de Riedmatten, “Generation of single photons with highly tunable wave shape from a cold atomic ensemble,” *Nat Commun* **7**, 13556 (2016).

[48] C. Yang, Z. Gu, P. Chen, Z. Qin, J. F. Chen, and W. Zhang, “Tomography of the Temporal-Spectral State of Subnatural-Linewidth Single Photons from Atomic Ensembles,” *Phys. Rev.*

Applied **10**, 054011 (2018).

- [49] R. Chinnarasu, C.-Y. Liu, Y.-F. Ding, C.-Y. Lee, T.-H. Hsieh, I. A. Yu, and C.-S. Chuu, “Efficient generation of subnatural-linewidth biphotons by controlled quantum interference,” Phys. Rev. A **101**, 063837 (2020).
- [50] B. Srivathsan, G. K. Gulati, B. Chng, G. Maslenikov, D. Matsukevich, and C. Kurtsiefer, “Narrow Band Source of Transform-Limited Photon Pairs via Four-Wave Mixing in a Cold Atomic Ensemble,” Phys. Rev. Lett. **111**, 123602 (2013).
- [51] M. Steiner, V. Leong, M. A. Seidler, A. Cerè, and C. Kurtsiefer, “Photon bandwidth dependence of light-matter interaction,” Opt. Express **25**, 6294-6301 (2017).
- [52] R. T. Willis, F. E. Becerra, L. A. Orozco, and S. L. Rolston, “Correlated photon pairs generated from a warm atomic ensemble,” Phys. Rev. A **82**, 053842 (2010).
- [53] R. T. Willis, F. E. Becerra, L. A. Orozco, and S. L. Rolston, “Photon statistics and polarization correlations at telecommunications wavelengths from a warm atomic ensemble,” Opt. Express **19**, 14632-14641 (2011).
- [54] D.-S. Ding, Z.-Y. Zhou, B.-S. Shi, X.-B. Zou, and G.-C. Guo, “Generation of non-classical correlated photon pairs via a ladder-type atomic configuration: theory and experiment,” Opt. Express **20**, 11433-11444 (2012).
- [55] Y.-S. Lee, S. M. Lee, H. Kim, and H. S. Moon , “Highly bright photon-pair generation in Doppler-broadened ladder-type atomic system,” Opt. Express **24**, 28083-28091 (2016).
- [56] C. Wang, C.-H. Lee, and Y.-H. Kim, “Generation and characterization of position-momentum entangled photon pairs in a hot atomic gas cell,” Opt. Express **27**, 34611-34617 (2019).
- [57] L. Zhu, X. Guo, C. Shu, H. Jeong, and S. Du, “Bright narrowband biphoton generation from a hot rubidium atomic vapor cell,” Appl. Phys. Lett. **110**, 161101 (2017).
- [58] X. Li, D. Zhang, D. Zhang, L. Hao, H. Chen, Z. Wang, and Y. Zhang, “Dressing control of biphoton waveform transitions,” Phys. Rev. A **97**, 053830 (2018).
- [59] Y. Liu, K. Li, S. Zhang, H. Fan, W. Li, and Y. Zhang, “Generation of correlated biphoton via four wave mixing coexisting with multi-order fluorescence processes,” Sci. Rep. **9**, 20065 (2019).
- [60] J. Mika and L. Slodika, “High nonclassical correlations of large-bandwidth photon pairs generated in warm atomic vapor,” J. Phys. B: At. Mol. Opt. Phys. **53**, 145501 (2020).
- [61] T. Jeong and H. S. Moon, “Temporal- and spectral-property measurements of narrowband

photon pairs from warm double- Λ -type atomic ensemble,” Opt. Express **28**, 3985-3994 (2020).

[62] G. Wang, Y.-S. Wang, E. K. Huang, W. Hung, K.-L. Chao, P.-Y. Wu, Y.-H. Chen, and I. A. Yu, “Ultranarrow-bandwidth filter based on a thermal EIT medium,” Sci. Rep. **8**, 7959 (2018).

[63] B. Kim, K.-T. Chen, C.-Y. Hsu, S.-S. Hsiao, Y.-C. Tseng, C.-Y. Lee, S.-L. Liang, Y.-H. Lai, J. Ruseckas, G. Juzeliūnas, and I. A. Yu, “Effect of laser-frequency fluctuation on the decay rate of Rydberg coherence,” Phys. Rev. A **100**, 013815 (2019).